Seismic Response Analysis of Silo-Stock-Foundation Interaction System

Shuwei Li[1, 2]* Wen Zhao[1] Zhiyu Guo[3]

1. School of Resources & Civil Engineering, Northeastern University, Shenyang, Liaoning, 110004, China
2. China Energy Engineering Group Co., Ltd., Beijing, 100022, China
3. China Energy Construction Group Heilongjiang Electric Power Design Institute Co., Ltd., Harbin, Heilongjiang, 150078, China

Abstract: To analyze the response law of silo-stock-foundation interaction system under seismic load, a dynamic equation of this interaction system was established. Furthermore, the dynamic characteristics of the silo-stock-foundation interaction system under different storage conditions were studied through numerical analysis. The displacement at the silo top was much greater than that at the silo bottom, while the vibration trend of the upper and lower silos on the same bus bar was similar. The acceleration response, displacement and stress response of the structure increased with the increase of the input seismic wave. Furthermore, the direction time responses of several typical silo parts were consistent. With increase in storage material, the acceleration peak of the silo and bulk material increased and then decreased. This indicates that the relative motion of the storage material and silo had a damping effect on the silo system. The maximum circumferential strain and equivalent stress of silos with different storage capacities were recorded at the variable section of silos (the top of funnel). The effective stress beneath foundations near silos was obviously higher than that far away from silos. These results can provide a reliable theoretical basis and reference values for mitigating silo structural failures under seismic load.

Keywords: silo-stock-foundation system; seismic response; dynamic characteristics; silo-stock-foundation interaction; seismic load; numerical analysis

***Corresponding Author:** Shuwei Li,School of Resources & Civil Engineering, Northeastern University, 11 Lane 3, Cultural District, Heping District, Shenyang, Liaoning, China Email: 18861770832@163.*com*

DOI: https://doi.org/10.30564/frae.v1i2.46

1. Introduction

Silo structures are widely used for the storage of various kinds of bulk materials[1-3] (Huachao Ding, 2016; Kunpeng Guo, 2016; Yichen Gao and Guozhi Qiu, 2017). Earthquakes are one of the main causes of silo instability,[4-5] [10-11] (Longfei Yuan et al., 2012; Yang Yu, 2012). Therefore, research on the dynamic characteristics of silos under earthquake excitation is of great practical significance. Domestic and foreign scholars have conducted several theoretical and experimental studies on the dynamic characteristics of silos,[6-8][12] (Chao Ma, 2008; Jinsuo Gao, 2009; Lujian Zhang, 2010; Yingwen Che, 2011; Xianping and Heng, 2011). However, most of these studies did not consider the interaction of silo-storage-foundation system, and focused only on the engineering mechanics characteristics of a single silo[9] (Guansheng Yin, 2002; Jianping Wang and Huang Yi, 2005; Mingping Wang, 2007). Furthermore, studies on the silo-stocking-foundation interaction system are limited and therefore the mechanism of this system is not clear. Since seismic load is one of the primary causes of silo structural instability, studying the dynamic characteristics of the silo-stock-foundation interaction system under seismic load is very important.

Combined with engineering practice, a silo storage foundation system was studied, and a dynamic characteristic model of the silo storage foundation system under different storage conditions was established. Through numerical analysis, the dynamic characteristics of the silo storage foundation system were studied further. The results of this study can provide a theoretical basis and reference values for the seismic design of silo structures that ensures safe operation under special conditions.

2. Basic Equations of Dynamic Model

The silo-storage-foundation interaction system can be regarded as a composite thin-walled cylindrical shell with one end fixed and the other end free. Figure 1 shows the cylindrical shell diagram and its stratification during external periodic load changes. During its movement, the cylindrical shell showed a displacement of each point in the cylindrical coordinate system with u, v, and was the three displacement components, which are simultaneously

a function of the spatial coordinates x, θ, r, and time t.

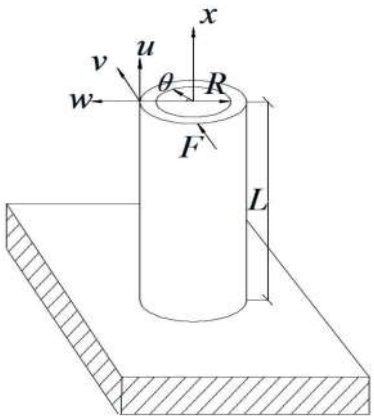

Figure 1. Model of A Circular Cylindrical Shell

2.1 Geometric Equations

The strain component at any point of a thin-walled cylindrical shell has the following relationship with the mid-plane strain, mid-plane bending deflection, and mid-plane distortion, respectively:

$$\varepsilon_x = \varepsilon_x^0 + z\chi_x \tag{1}$$

$$= \quad + \tag{2}$$

$$\varepsilon_{x\theta} = \varepsilon_{x\theta}^0 + z\chi_{x\theta} \tag{3}$$

where ε_x^0, ε_θ^0, and $\varepsilon_{x\theta}^0$ are the film strain components of the middle curve, χx and χθ represent the mid-plane bending deflection, χxθ is the mid-plane twist, and z is the distance from any point on the shell to the middle.

According to the Donnell shell theory, the first-order derivative nonlinearity of the normal deflection is considered in the relationship between the mid-surface strain and displacement.

$$\varepsilon_x^0 = \frac{\partial u}{\partial x} + \underline{\frac{1}{2}\left(\frac{\partial w}{\partial x}\right)^2} \tag{4}$$

$$\varepsilon_\theta^0 = \frac{1}{R}\left(\frac{\partial v}{\partial \theta} + w\right) + \underline{\frac{1}{2}\left(\frac{\partial w}{R\partial \theta}\right)^2} \tag{5}$$

$$\varepsilon_{x\theta}^0 = \frac{\partial v}{\partial x} + \frac{1}{R}\frac{\partial u}{\partial \theta} + \underline{\frac{\partial w}{\partial x}\frac{1}{R}\frac{\partial w}{\partial \theta}} \tag{6}$$

In Equations 4–6, the underlined items represent nonlinear terms.

In the Donnell nonlinear shell theory, the mid-plane bending strain component remains linear:

$$\chi_x = -\frac{\partial^2 w}{\partial x^2} \tag{7}$$

$$\chi_\theta = -\frac{1}{R^2}\frac{\partial^2 w}{\partial \theta^2} \tag{8}$$

$$\chi_{x\theta} = -\frac{2}{R}\frac{\partial^2 w}{\partial x \partial \theta} \tag{9}$$

2.2 Physic Equations

Considering the elastic modulus of the composite material with vibration frequency changes, it can be obtained:

$$E_1(\omega) = E_2(\omega) = E_3(\omega) = 2.5751\times10^9 + \frac{2\times3.2283\times10^{12}}{\pi}\times\left[\frac{238.62}{4\times(\omega/2\pi - 0.46787)^2 + 238.62^2}\right] \tag{10}$$

$$E_4(\omega) = 5.04289\times10^8 + 9.2387\times10^9 \times e^{-0.0064\omega/2\pi} \tag{11}$$

The physical equation of layer K of the isotropic laminated shell is given as

$$\begin{bmatrix}\sigma_x\\ \sigma_\theta\\ \tau_{x\theta}\end{bmatrix}_k = \begin{bmatrix}Q_{11} & Q_{12} & 0\\ Q_{21} & Q_{22} & 0\\ 0 & 0 & Q_{66}\end{bmatrix}_k \begin{bmatrix}\varepsilon_x\\ \varepsilon_\theta\\ \varepsilon_{x\theta}\end{bmatrix}_k \tag{12}$$

Where Q_i^j is the reduced stiffness matrix, and the element expression is given as

$$(Q_{11})_k = (Q_{22})_k = E_k(\omega)/(1-\mu_k^2) \tag{13}$$

$$(Q_{12})_k = (Q_{21})_k = E_k(\omega)\cdot\mu_k/(1-\mu_k^2) \tag{14}$$

$$(Q_{66})_k = E_k(\omega)/2(1+\mu_k) \tag{15}$$

Where Ek(ω) is the k-th elastic modulus and μk is the k-th layer of Poisson's ratio.

2.3 Dynamic Balance Equations

According to the principle of D'Alembert, the dynamic equilibrium equation of a laminated composite cylindrical shell can be established as

$$\frac{\partial N_x}{\partial x} + \frac{1}{R}\frac{\partial N_{x\theta}}{\partial \theta} - \sum_{k=1}^{4}\rho_k(z_k - z_{k-1})\frac{\partial^2 u}{\partial t^2} = 0 \tag{16}$$

$$\frac{1}{R}\frac{\partial N_\theta}{\partial \theta} + \frac{\partial N_{x\theta}}{\partial x} + \frac{Q_\theta}{R} - \sum_{k=1}^{4}\rho_k(z_k - z_{k-1})\frac{\partial^2 v}{\partial t^2} = 0 \tag{17}$$

$$\frac{\partial Q_x}{\partial x} + \frac{1}{R}\frac{\partial Q_\theta}{\partial \theta} - \frac{1}{R}N_\theta + N_x\frac{\partial^2 w}{\partial x^2} + \frac{N_\theta}{R^2}\frac{\partial^2 w}{\partial \theta^2} + \frac{2N_{x\theta}}{R}\frac{\partial^2 w}{\partial x \partial \theta} - \sum_{k=1}^{4}\rho_k(z_k - z_{k-1})\frac{\partial^2 w}{\partial t^2} - c\frac{\partial w}{\partial t} - q_r = 0 \tag{18}$$

Where can be presented as

$$Q_x = \frac{1}{R}\frac{\partial M_{x\theta}}{\partial \theta} + \frac{\partial M_x}{\partial x} \tag{19}$$

$$Q_\theta = \frac{\partial M_{x\theta}}{\partial x} + \frac{1}{R}\frac{\partial M_\theta}{\partial \theta} \tag{20}$$

3. Numerical Calculation

3.1 Project Overview

The Shenyang Jinshan Thermal Power Heating Project needs setting up of 5 million ton silos with a diameter and height of 22 and 39.730 m, respectively. According to the specification, the silo was identified as a deep warehouse, and lignite coal with a bulk density of 10kN/m3 was used. The seismic fortification intensity was 7 degrees; the basic seismic acceleration was designed as 0.10 g; the seismic structure was fortified at 7°; and the seismic level was 2. The structure received a structural safety rating of 2, fire rating of 2, foundation design grade B, and had a design life of 50 years. Medium-coarse sand was used as the base holding layer is, and the silo warehouse wall was reinforced by pouring concrete. The structure of the cross-section shown is shown in Figure 2.

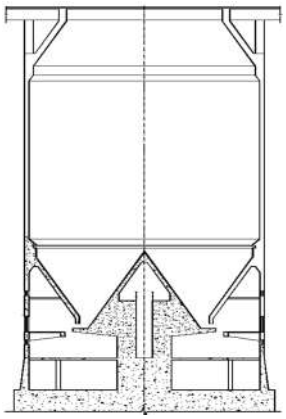

Figure 2. Sketch Map of the Profile of Silo

3.2 Material Parameters

HRB335 steel is selected for the silo steel, and the strength of concrete is C40. The silos were filled from the top to bottom of the foundation with soil (1 m), silty clay (5 m), coarse sand (2 m), and gravel sand. The base holding layer was medium-coarse sand, and the surface fill layer was very thin. For simplified calculation, the mechanical parameters of the material are equivalent to silty clay. The lignite was stored in the silos.

3.3 Contact and Boundary Conditions

The model uses smoothed particle hydrodynamics particles as nodes, which are in point-to-surface contact with the silo wall. The dynamic friction coefficient between storage material and silo wall is 0.5, and the static friction coefficient is 0.9.

The upper surface of the foundation soil is a free boundary condition. The surrounding of the foundation soil is set as the nonreflecting boundary condition to avoid the influence of the reflected tensile wave on the calculation results and to restrain the normal displacement of the boundary surface. The normal displacement and rotational freedom of the ground surface node restraint release two horizontal displacement components.

3.4 Finite Element Model

In this study, the finite element software ANSYS/LS-DYNA3D was used to build the silo-foundation model according to the actual project size of 1:1. As shown in Figure 3, the bonding between the silo and foundation is used to ensure the continuity of the displacement. The total is divided into 32,640 units and 36,656 nodes. The Lanzhou wave was selected as the input seismic wave in the numerical simulation, the time history curve and spectrum curve of the Lanzhou wave are shown in Figure 4.

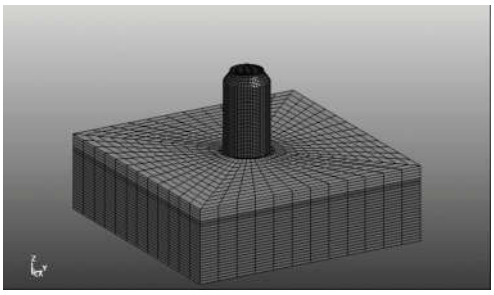

Figure 3. Schematic Diagram of the Model

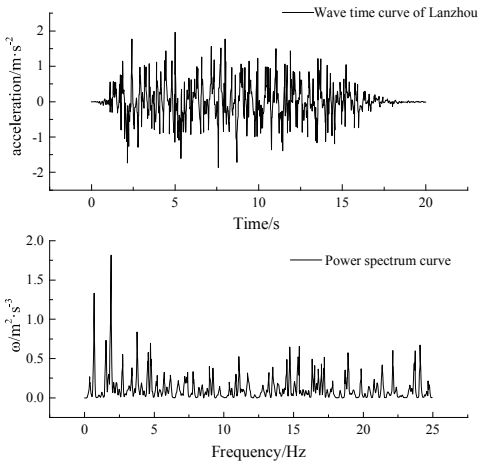

Figure 4. The Time History Curve and Spectrum Curve of Lanzhou wave

3.5 Seismic Response Analysis

3.5.1 Time History Analysis of Displacement and Acceleration

Under the action of seismic waves, the displacement and acceleration peak curves of the nodes at the top of the silo,

the junction of the silo, and the ground and top of the storage material, are shown in Figure 5.

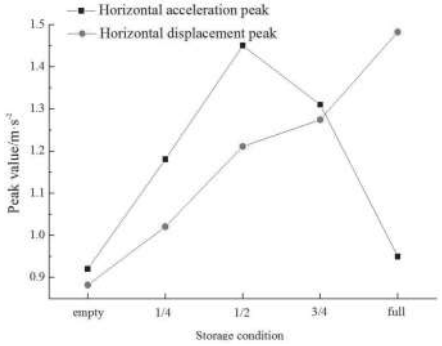

Figure 5 (a). Time Curves of Displacement and Acceleration at the Model's Monitoring Points

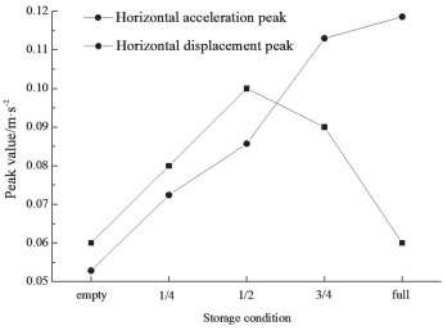

Figure 5 (b). Time Curves of Displacement and Acceleration at the Model's Monitoring Points of Silo-to-Ground Interface

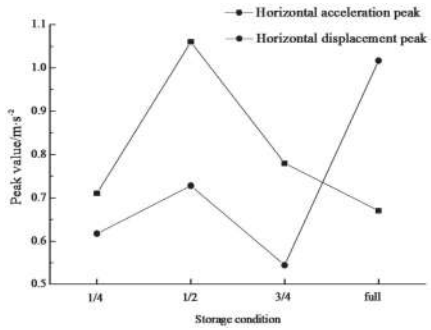

Figure 5 (c). Time History Curves of Nodal Displacements and Acceleration at the Top of the Storage Material

The analysis shows that the displacement at the top of the silo is far greater than that at the bottom, and the trend of the upper and lower silos in the same bus bar is similar. The larger the input seismic wave, the greater are the structural acceleration response, displacement deformation, and stress response. From the point of view of the whole structure, the movement directions of the time histories of several typical silos are consistent, indicating that the entire body of the warehouse is swinging.

With the increase in storage, the peak acceleration of silos and bulk materials first increases, and then decreases, indicating that the relative movement of the storage and silos has a damping effect on the silo system.

3.5.2 Silo and Storage Material Effective Stress Analysis

Figure 6 shows the effective stress maps of silos and silos under different storage conditions when the displacement of silo nodes and storage nodes reaches their peak.

Figure 6 (a). Silo Effective Stress Cloud Chart under the Condition of Short Position

Figure 6 (b). Effective Stress Cloud Chart of Foundation under Empty Condition

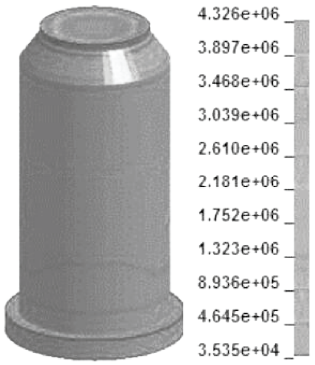

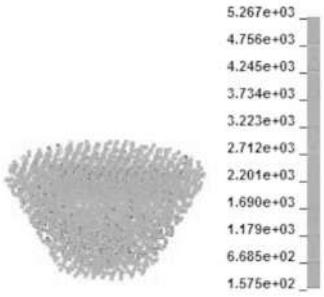

Figure 6 (c). Effective Stress Cloud Chart of Silo and Storage under 1/4 Storage

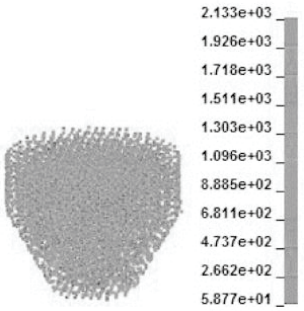

Figure 6 (d). Effective Stress Cloud Chart of Silo and Storage under 1/2 Storage

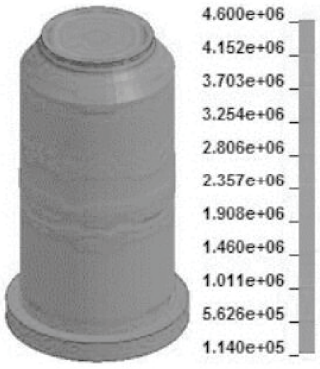

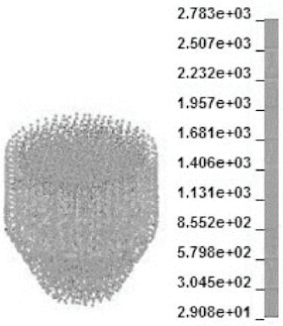

Figure 6 (e). Effective Stress Cloud Chart of Silo and Storage under 3/4 Storage

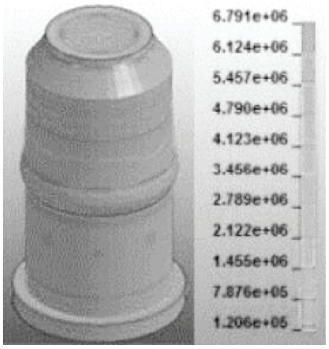

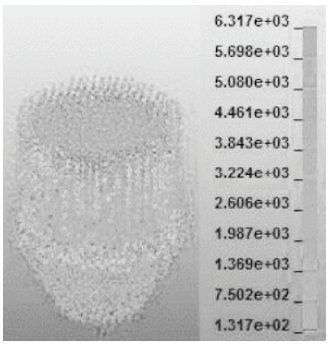

Figure 6 (f). Effective Stress Cloud Chart of Silo and Storage under Full Storage

Figure 6. Effective Stress Cloud Chart for Silos and Storage Material under Different Storage Conditions

As can be seen from Figure 6, the maximum circumferential strain and the maximum equivalent stress of silos with different storage capacity all appear at the variable section of silos, namely the top of funnels, and should be strengthened in the design of silos. The effective stress in the subgrade of the silo foundation is obviously higher than that in the far zone, and the foundation of the base area should be strengthened to avoid the instability of the foundation.

4. Engineering Examples of Optimal Design

4.1 Silo Structure Optimization Background

The test methods mostly calculated the moment of the basement by measuring the hoop strain and the vertical strain at the bottom of the silo test model, combined with the elastic modulus and Poisson's ratio from the model. In the numerical model, a node along the Z-axis of the force component was multiplied by the node at the base of the silos, formed by the central X-axis component, and then all the results of the node were used to obtain the value of the base moment. "Code for Design of Reinforced Concrete Silos" GB 50077-2003 states that the moment of the base can be calculated as follows:

$$M_{Ek}=\alpha_1 (G_{sk}h_s+G_{mk}h_m) \quad (21)$$

where, α_1 is the horizontal seismic influence coefficient of the basic natural vibration period of the structure, G_{sk} is the representative value of the silo weight gravity load, G_{mk} is the representative value of the total weight of the gravity load, M_{Ek} is the standard value of the moment at the bottom of the silo, h_s is the height of the center of gravity of the silo, and h_m is the total weight at the center of gravity height.

A comparison of the model test, numerical simulation, and standard calculations of the bending moment of the silo base under different loads is listed in Table 1.

Table 1. Comparison Results of Base Bending Moment Values of Silos

Base moment (N•m)	Short positions	1/4 positions	1/2 positions	3/4 positions	Full positions
Test results	950	1223	1587	1963	2274
Simulation results	1981	2341	2872	3256	3899
Specification calculation	1633	2018	2295	2684	3026

As can be seen from Table 1, the formula given by the specification is too conservative and will result in greater material waste. The original design can therefore be optimized using our method.

4.2 Silo Structure Optimization

4.2.1 Basic Optimization

The silo is a tube-supported reinforced concrete silo, the original design of the base plate is square, the base plate thickness is 2.5 m, and the base depth is -5.77 m. After optimization, the base plate was changed to a circular shape. The thickness of the base plate was optimized to 2.3 m by reducing the thickness by 200 mm. The base depth was increased to -5.77 m and the depth of the base was reduced by 200 mm.

4.2.2 Roof Thickness Optimization

The thick structure of the top of the silo not only causes material wastage, but also the excessive weight of the top of the silo will increase the center of mass of the silo structure, increase the rigidity of the silo, and thus increasing the natural frequency of the silo and intensifying the displacement of the top of the silo under the influence of a horizontal earthquake, compromising structural safety. To this end, the thickness of the roof structure after optimization was reduced from 2.0 m to 0.8 m. The top of the silo warehouse is designed as inverted conical shell structure. The silo roof reinforcement was calculated by SILO alone to reduce the height of the silo wall and reduce the amount of reinforcement and the amount of concrete in the silo wall.

4.2.3 Silo Reinforcement Optimization

The PKPM silo module was used to optimize the model. The calculations showed that the spacing between the annular steel bars in the cylinder wall could be optimized from 125 mm to 135 mm, which greatly reduces the amount of steel used. Figure 7 and Figure 8, respectively show the optimal design of the silo structure reinforcement and the resulting crack model.

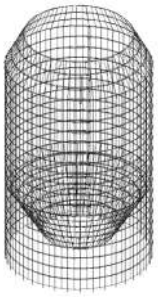

Figure 7. Structure Reinforcement Diagram

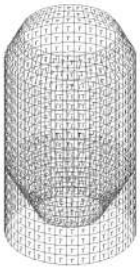

Figure 8. Crack Map

4.2.4 Other Construction Measures to Optimize

Considering to the change of temperature difference in winter in Shenyang and the mechanical properties of concrete under this temperature, the thermal insulation of the outer wall of the silo was removed.

4.3 Silo Optimization Results Analysis

4.3.1 Comparison of Engineering Quantity before and after Optimization

The results of the comparison of silos before and after the optimization are shown in Table 2. As can be seen from table 2, the original design of a single silo cost about 50

million yuan, and the cost of a single silo was reduced by 10 million yuan by optimizing the design. The total cost of the whole project would therefore be reduced by nearly 50 million yuan, conserving the quality of the project and achieving favorable economic benefits.

Table 2. Comparison of Engineering Quantity before and after Optimization of Silo

Optimization indicators	Unit	Before optimization	After optimization	Change due to optimization
Amount of steel used	T	2372	1935	-437
Amount of concrete used	m^3	17367	14332	-3035
Tube wall outside the insulation (MU7.5 porous sintered brick)	m^3	2875	0	-2875

4.3.2 Analysis of Silo Settlement after Optimization

The 5-tonne silo of the Shenyang Jinshan Thermal Power Plant 2×200 MW "Large Generation" Heating Project coal handling system has been operating safely for nearly 10 years since it was first put into production. No cracks have occurred in the silo wall, and the supporting structure has not affected normal production. The foundation settlement stabilized 12 months after it was put into operation, with no uneven settlement. The settlement value peaked at 33 mm, meeting the requirements of relevant specifications. The settlement volume two years after commissioning is shown in Figure 9. This proves the conservativeness of internal force calculation and the rationality of silo optimization under the action of horizontal earthquakes. The optimal design methods presented here should therefore be popularized and widely applied.

5. Conclusion

The silo displacement of the silo top is far greater than that of the bottom, and the trend of the upper and lower silos in the same bus bar is similar. The structure acceleration response, displacement deformation and stress response increase with the increase of input seismic amplitude.

From the whole structure, several typical parts of silos of the time-course response to the movement of the same direction, indicating that the overall swinging warehouse body. With the increase of storage, the peak acceleration of silos and bulk materials first increases and then decreases, indicating that the relative movement of storage silos and silos has a damping effect on the silo system.

The maximum hoop strain and the maximum equivalent stress of silos with different storage capacities appeared at the top of the funnel at the variable cross section of the silo, and the effective stress in the silo near the foundation was significantly higher than that in the far zone.

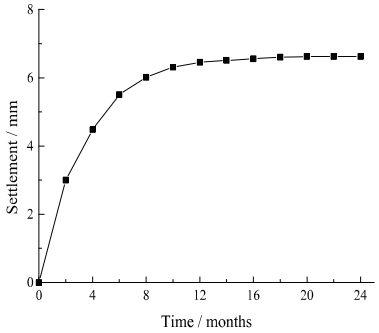

Figure 9. Settlement Curve of Silo

References

[1] Yingwen Che. Research on the Stress Situation and Stability of Silo[D].Wuhan University of Technology,2011. (in Chinese)

[2] Huachao Ding. Study on Mechanical Performance Analysis and Design Optimization of Viaduct Silo[D].Zhengzhou University,2016. (in Chinese)

[3] Jinsuo Gao. Analysis of Floor Type Steel Silo Earthquake[D].Xi'an University Of Architecture And Technology,2009. (in Chinese)

[4] Yichen Gao, Guozhi Qiu. The Storage of Material Parameters on Horizontal Earthquake Effect of Silo[J].Science Technology and Engineering, 2017, 17(01): 79–84. (in Chinese)

[5] Kunpeng Guo. Distribution Mechanism of Silo Storage Pressure and Seismic Vulnerability Study[D]. Beijing Jiaotong University,2016. (in Chinese)

[6] Chao Ma. Silo Structure-Dynamic Calculation of Foundation Iinteraction[D]. Chang'an University, 2008. (in Chinese)

[7] Jianping Wang, Yi Huang. The Present Situation and Prospect of the Aseismic Study of the Silo Structure in China[J].Industrial Construction, 2005,(04): 79-81+90. (in Chinese)

[8] Mingping Wang, Yuchuan Li, Wei Liu. Calculation of the Vibration Period and Seismic Action of a Silo with a Barn[J].Journal of Vibration and Shock, 2007, (08): 5-8+165. (in Chinese)

[9] Guansheng Yin. Static and Dynamic Study of Silo Structure Considering Structure Foundation Interaction[D]. Xi'an University Of Architecture and Technology,2002. (in Chinese)

[10] Yang Yu. Seismic Response Analysis of Reinforced Concrete Cylindrical Silo Wall Structure[D].Xi'an University of Science and Technology,2012. (in Chinese)

[11] Longfei Yuan, Xiaowen Li, Guoliang Bai, et al. Seismic Response Analysis of Prestressed Concrete Round Coal Silo[J].World Earthquake Engineering, 2012, 28 (01): 81-86. (in Chinese)

[12] Lujian Zhang. Experimental Research on Seismic Shaking Table Simulation of Cylinder Bearing Type Vertical Cylinder Group Structure Model[D].Henan University of Technology, 2010. (in Chinese)